European Journal of Medicinal Chemistry 66 (2013) 438–449

Contents lists available at SciVerse ScienceDirect

European Journal of Medicinal Chemistry

journal homepage: http://www.elsevier.com/locate/ejmech

Original article

Identification of novel chromone based sulfonamides as highly potent and selective inhibitors of alkaline phosphatases

Mariya al-Rashida [a,**], Rabia Raza [b], Ghulam Abbas [c], Muhammad Shakil Shah [b], George E. Kostakis [d], Joanna Lecka [e,f], Jean Sévigny [e,f], Muhammad Muddassar [g], Constantina Papatriantafyllopoulou [h], Jamshed Iqbal [b,*]

[a] Department of Chemistry, Forman Christian College (A Chartered University), Ferozepur Road, 54600 Lahore, Pakistan
[b] Department of Pharmaceutical Sciences, COMSATS Institute of Information Technology, Abbottabad 22060, Pakistan
[c] Interdisciplinary Research Centre in Biomedical Materials (IRCBM), COMSATS Institute of Information Technology, Lahore 54590, Pakistan
[d] Institute of Nanotechnology, Karlsruhe Institute of Technology, Hermann-von-Helmholtz Platz 1, 76344 Eggenstein-Leopoldshafen, Germany
[e] Centre de Recherche en Rhumatologie et Immunologie, CHU de Québec, Québec, QC, Canada
[f] Département de Microbiologie-Infectiologie et d'Immunologie, Faculté de Médecine, Université Laval, Québec, QC, Canada
[g] Zhang Initiative Research Unit, Advanced Science Institute, RIKEN, 2-1 Hirosawa, Saitama, Wako 351-0198, Japan
[h] Department of Chemistry, University of Cyprus, CY-1678 Nicosia, Cyprus

ARTICLE INFO

Article history:
Received 14 April 2013
Received in revised form
7 June 2013
Accepted 10 June 2013
Available online 19 June 2013

Keywords:
Alkaline phosphatase inhibitors
Ecto-5′-nucleotidase inhibitors
Chromones
Sulfonamides
Molecular docking
Structure activity relationships (SARs)

ABSTRACT

A new series of structurally diverse chromone containing sulfonamides has been developed. Crystal structures of three representative compounds (**2a**, **3a** and **4a**) in the series are reported. All compounds were screened for their inhibitory potential against alkaline phosphatases (ALPs). Two main classes of ALP isozymes were selected for this study, the tissue non-specific alkaline phosphatase (TNALP) from bovine and porcine source and the tissue-specific intestinal alkaline phosphatases (IALPs) from bovine source. All sulfonamide compounds had a marked preference for IALP (K_i, up to 0.01 ± 0.001 μM) over TNALPs. Kinetics studies of the compounds showed competitive mode of inhibition. Molecular docking studies were carried out in order to characterize the selective inhibition of the compounds. An additional interesting aspect of these chromone sulfonamides is their inhibitory activity against ecto-5′-nucleotidase enzyme.

1. Introduction

Alkaline phosphatases (ALPs, EC 3.1.3.1) are dimeric enzymes that catalyze hydrolysis of phosphomonoesters at an alkaline pH [1]. Different isozymes of alkaline phosphatases are grouped under two categories; the tissue specific alkaline phosphatases (placental PALP, germ cell GALP, intestinal IALP) and tissue non-specific alkaline phosphatase (TNALP). The exact physiological function of these enzymes is obscure [2]. A vital role of ALP in biomineralization has been known for a long time by virtue of its high concentrations in mineralizing tissues. Hessle et al. [3] have provided evidence for the regulatory role of ALP and plasma cell membrane glycoprotein-1 (PC-1) in bone mineralization via modulation of extracellular PP_i levels. The concerted relation of TNALP and PC-1 is an inverse one, TNALP hydrolyzes PP_i (a potent inhibitor of mineralization) and PC-1 is responsible for maintaining sufficient levels of extracellular PP_i. Together TNALP and PC-1 are important for balanced bone formation. Deficiency of TNALP due to gene mutation is responsible for the severe disorder of bones and elevated levels of extracellular PP_i [4]. On the other hand unwanted deposition of hydroxyapatite (HA) along with other forms of calcium phosphate in soft tissues is termed hydroxyapatite deposition disorder (HADD) [5]. It has been suggested that the pool of P_i required for HA deposition is provided by TNALP via hydrolysis of PP_i and nucleoside triphosphates. Another major source of phosphate supply is through intestinal absorption where IALP may play a role. IALP has also been suggested to be involved in lipid absorption as a parallel increase has been observed in triacylglycerol concentration and IAP activity, during fat absorption in thoracic duct lymph [6,7].

Abbreviations: ALP, alkaline phosphatase; IALP, intestinal alkaline phosphatase; TNALP, tissue non specific alkaline phosphatase; ecto-5′-NT, ecto-5′-nucleotidase.

* Corresponding author. Tel.: +92 992 3835916; fax: +92 992 383441.
** Corresponding author. Tel.: +92 3432106432; fax: +92 (42) 9923 0703.
E-mail addresses: maria_al_rashida@hotmail.com (M. al-Rashida), jamshediqb@gmail.com, drjamshed@ciit.net.pk (J. Iqbal).

0223-5234/$ – see front matter © 2013 Elsevier Masson SAS. All rights reserved.
http://dx.doi.org/10.1016/j.ejmech.2013.06.015

TNALP is an important therapeutic target for modulation of biomineralization. Inhibition of TNALP may have advantages in treatment of HADD, tumor calcification and vascular mineralization [8]. IALP was found to be over-expressed in mucosal biopsies in patients with inflammatory bowel disease specifically Crohn's disease [9]. Here the role of IALP selective inhibitors as potential therapeutic agents cannot be over looked. Because of high homology between tissue specific IALP and TNALP, a very few selective inhibitors of IALP have been reported; moreover inhibition constants of these inhibitors are relatively high and poorly selective [10–12]. Selective sulfonamide inhibitors of IALP are still lacking in literature, the only other aryl sulfonamides known as selective inhibitors are those of TNALP described by Dahl et al. [13]. This prompted us toward the development of potent and selective chromone based sulfonamide inhibitors of TNALP and IALP.

2. Results and discussion

2.1. Chemistry

Depending on the sulfonamide nitrogen substitution, two types of compounds have been prepared. Compounds of type **A**, containing N-un-substituted sulfonamide moiety (–RSO_2NH_2, Scheme 1; **1a**–**1e**, **2a**–**2e**, **3a**–**3e**). The compounds of type **B** (Scheme 2; **4a**–**4f**) were similarly prepared by reacting 3-formylchromones with N-heteroaryl substituted sulfonamides and had the general formula –RSO_2NHR'.

Owing to the presence of three electron deficient centers (C2, C3 and C4) in the molecule of 3-formylchromone (3-FC), the reactions of 3-FC with primary amines do not always yield Schiff base products. Ethanol is sufficiently nucleophilic and adds into the C2–C3 olefinic bond of chromone without causing ring cleavage. Chromone containing sulfonamide enamines were therefore obtained. Compounds **1a**–**1e** and **2a**–**2e**, formed via reaction of 3-FC with 4- and 3-ABS respectively, have already been reported by us [14–16]. When 2-ABS was reacted with 3-formylchromone (**3a**), 6-fluoro-3-formylchromone (**3b**) and 6-bromo-3-formylchromone (**3c**), a benzothiadiazine ring was formed. However, when 6,8-dibromo-3-formylchromone (**3d**) and 6-ethyl-3-formylchromone (**3e**) were reacted with 2-ABS, no ringed product was obtained and the structures were essentially similar to those obtained via reaction of 4- and 3-ABS. Single crystals suitable for analysis by X-ray diffraction were obtained for compounds **2a**, **3a** and **4a**, their crystal structures are reported here (Table 1) along with molecular diagrams (Figs. 1–6).

2.2. Enzyme inhibition studies (ALP, ecto-5′-NT) and SAR

The synthesized compounds were tested for their inhibitory potencies against two major groups of alkaline phosphatases i.e.

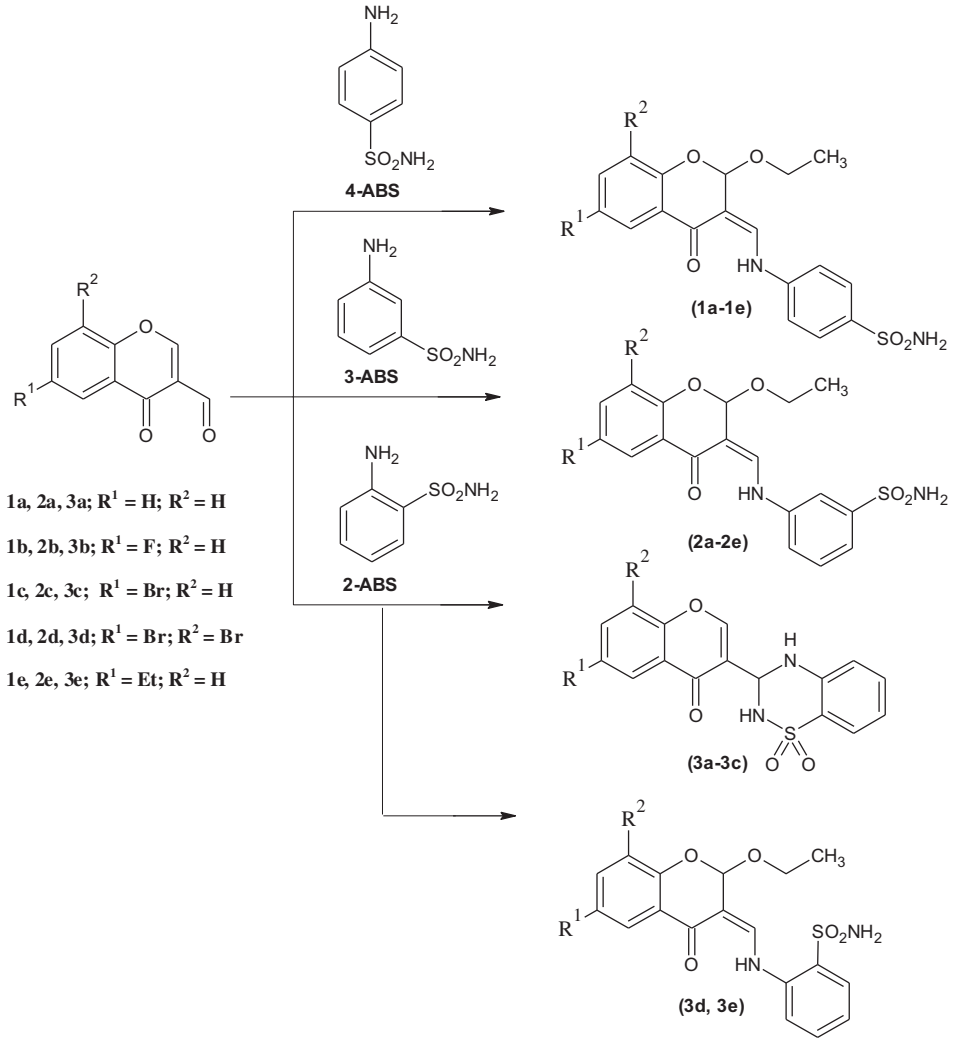

Scheme 1. Synthesis of compounds **1a**–**1e**, **2a**–**2e** and **3a**–**3e**.

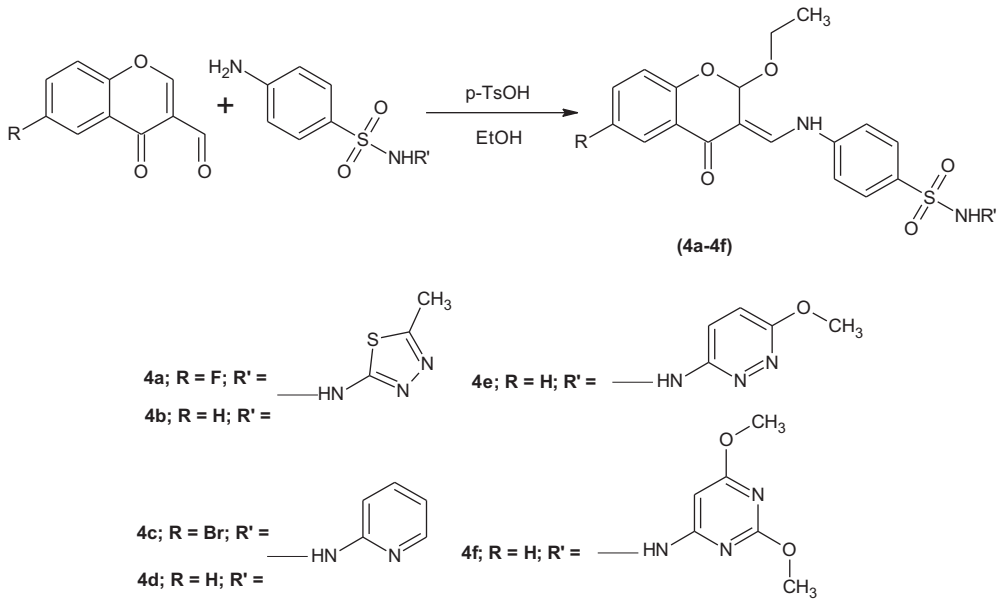

Scheme 2. Synthesis of compounds **4a**–**4f**.

Table 1
Summary of data collection and refinement parameters for compounds **2a**, **3a** and **4a**.

Compound	**2a**	**3a**	**4a**
Formula	$C_{18}H_{17}N_2O_5S$	$C_{16}H_{10}N_2O_4S$	$C_{23}H_{19}FN_4O_6S_2$
Formula weight	373.40	326.32	530.54
Crystal size	0.14 × 0.10 × 0.07	0.17 × 0.10 × 0.04	0.34 × 0.25 × 0.18
Crystal system	Monoclinic	Monoclinic	Monoclinic
Space group	*C*2/*c*	$P2_1/c$	$P2_1/n$
Unit cell dimensions			
a [Å]	25.8629 (19)	15.0557 (16)	4.9031 (2)
b [Å]	8.4035 (6)	7.0036 (5)	31.9121 (14)
c [Å]	15.7334 (10)	13.9873 (15)	16.4915 (8)
β [deg]	98.879 (7)°	113.760 (13)°	93.888 (3)°
V [Å^3]	3378.5 (4)	1349.9 (2)	2574.5 (2)
Z	8	4	4
Density (Dx Mg m^{-3})	1.468	1.606	1.369
F(000)	1560	672	1096
T [K]	100	100	296
μ(Mo-Kα) [mm^{-1}]	0.23	0.26	0.259
θ range [°]	2.8–28.9	2.9–29.1	2.6–28.4
h	−30 → 28	−17 → 17	−6 → 6
k	−9 → 9	−6 → 8	−42 → 41
l	−18 → 18	−16 → 11	−20 → 21
Absorption correction	Multi-scan	Multi-scan	Multi-scan
Measured reflections	8321	4843	20,520
Independent reflections	2965	2385	6408
R_{int}	0.056	0.065	0.0899
Parameters	251	216	290
Max. difference peak/hole [e Å^{-3}]	0.91/−0.36	2.35/−0.72	0.42/−0.28
S	1.07	1.26	0.92
Reflections with $I > 2\sigma(I)$	2525	1914	2456
$R[F^2 > 2\sigma(F^2)]$	0.047	0.109	0.055
$wR(F^2)$	0.123	0.317	0.168

tissue specific and tissue non specific alkaline phosphatase. Bovine intestinal ALP was used as tissue specific ALP while two sources for TNALP were used that are porcine kidney and bovine kidney. The results showed that all compounds exhibited almost comparable inhibition on both TNALPs and were generally much more potent and selective toward IALP. With the only exception of few compounds like **3c**, **2a**, **2b** and **4b** (for which there was almost comparable inhibition against both IALP and TNALPs), all other compounds have shown a marked preference for IALP over both TNALPs (Table 2). A graphical representation emphasizing on selective inhibition of bovine IALP over TNALP inhibition for compounds of type A (Fig. 7) and type B (Fig. 8) is given. Among compounds of type **A**, IALP inhibition activities of both *m*- and *p*-sulfonamide compounds were increased many fold upon substitution of chromone ring. Consequently **1a** and **2a** were weaker IALP inhibitors as compared to other compounds containing substituted chromone rings. The effect of halogenation of chromone ring on ALP activity was significant.

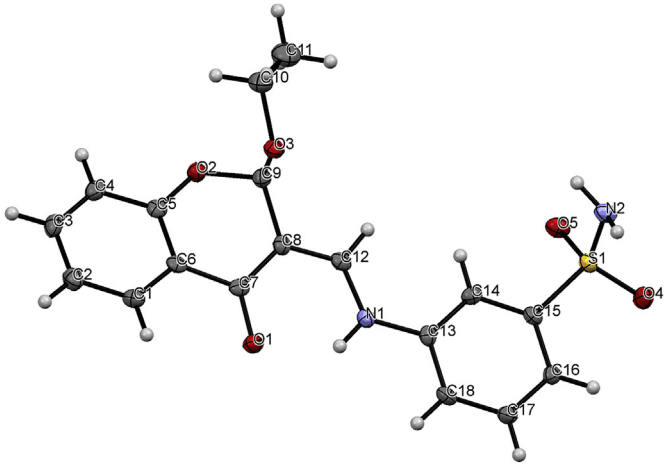

Fig. 1. ORTEP plot of **2a** showing atom labeling. Thermal ellipsoids are drawn at 50% probability level.

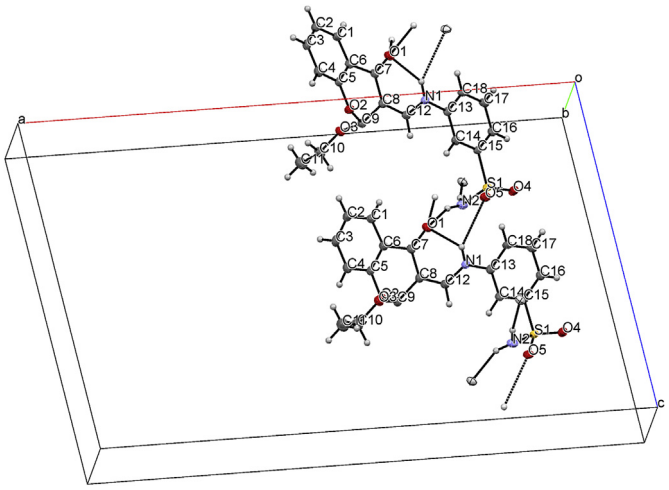

Fig. 2. Molecular packing diagram of **2a**.

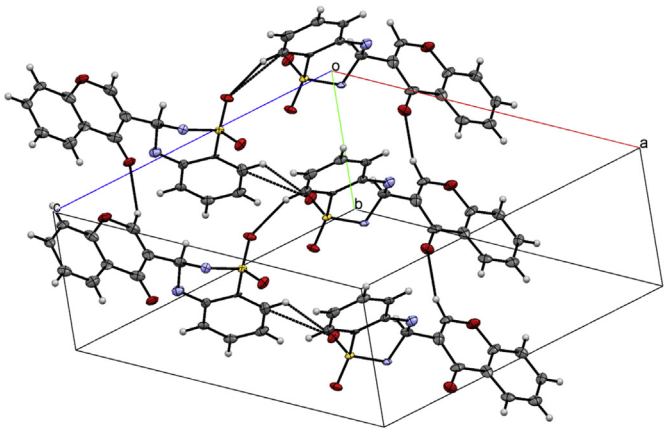

Fig. 4. Molecular packing diagram of **3a**.

When SO_2NH_2 group was at meta position, 6,8-di-substitution on chromone ring was preferred, hence compound **2d** was most potent IALP inhibitor among m-SO_2NH_2 containing compounds. The IALP inhibition tendency decreased significantly when bulky groups at 6-position of chromone ring were substituted by relatively compact groups, hence activity decreased in the order Et > Br > F ≫ H. Similar trends were observed for p-SO_2NH_2 containing compounds. In general bulky substituents at 6-position of chromone ring were preferred. Hence bromine containing **1c** was more active than fluorine containing **1b**. However, in contrast to m-series, in p-SO_2NH_2 containing compounds simultaneous substitution at 6 and 8 position of chromone ring resulted in decreased IALP inhibition. The least active compound in this series was **1a** which contained no substitution at chromone ring. Among compounds derived from 2-ABS (**3a**–**3e**), compound **3c** was most active IALP inhibitor followed by **3a**. Compounds in this series were also found to selectively inhibit bovine IALP over bovine TNALP. A comparison of concentration response curve of **3c** against bovine IALP, bovine TNALP and porcine TNALP is represented in Fig. 9.

Compounds of type **B** (**4a**–**4f**) with N-substituted sulfonamide group were also found be selective inhibitors of IALP over TNALP. Fluorine containing compound **4a** was most active. However when the fluorine was replaced by a hydrogen atom in **4b**, a decrease in IALP inhibition was observed. Compounds **4e** and **4f** inhibited IALP at a similar degree, but had different level of TNALP inhibition.

An interesting inference, regarding selective inhibition can be drawn from the structure activity relationship studies of p-SO_2NH_2 containing compounds (**1a**–**1e**). For all compounds in this series, substituents at 6-position of chromone ring caused a significant decrease in bovine TNALP inhibition. For these compounds 6-substitution at the chromone ring not only caused a decrease in bovine TNALP inhibition but at the same time also caused a significant increase in IALP inhibition (Table 2). This behavior is epitomized by comparing **1a** (potent TNALP inhibitor; weak IALP inhibitor) and its 6-fluoro analog **1b** (potent IALP inhibitor; weak TNALP inhibitor) (Fig. 10). This important SAR consideration can be a prolific lead in design of isozyme selective ALP inhibitors from this class of compounds. For the rest of the series **2a**–**2e**, **3a**–**3e** and **4a**–**4f**, 6-substitution at chromone ring did cause an average decrease in bovine TNALP inhibition, but the trend is not unanimous for all compounds, for example compounds **2b**, **2d**, **2e**, **3c** and **4b** did not show this behavior.

In order to characterize the mechanism of inhibition, double reciprocal plots of substrate concentration (mM^{-1}) and initial velocity were plotted for most potent inhibitor (**3c**) against CIALP. Enzyme kinetics was determined by evaluating the effect of 0, 100 and 300 nm of **3c**. A direct linear relationship in the K_m value and inhibitor concentration was observed i.e. K_m value increased with increasing inhibitor concentration. However V_{max} value remained unaffected in the absence and presence of inhibitors. Thus, it was inferred that both the compounds showed competitive inhibition. Double-reciprocal plot of the inhibition kinetics of **3c** is shown in Fig. 11.

Since the compounds prepared by us showed excellent potential to inhibit metal containing ALP which hydrolyzes phosphomonoesters, it was hypothesized that these compounds could also act

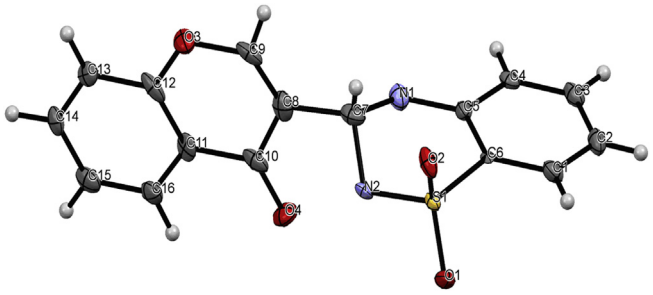

Fig. 3. ORTEP plot of **3a** showing atom labeling. Thermal ellipsoids are drawn at 50% probability level.

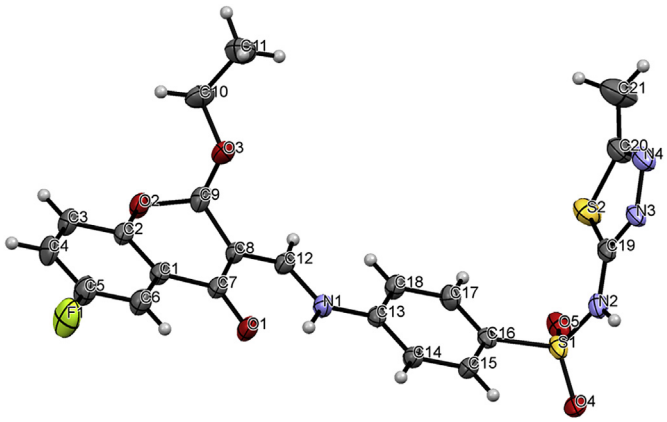

Fig. 5. ORTEP plot of **3a** showing atom labeling. Thermal ellipsoids are drawn at 30% probability level.

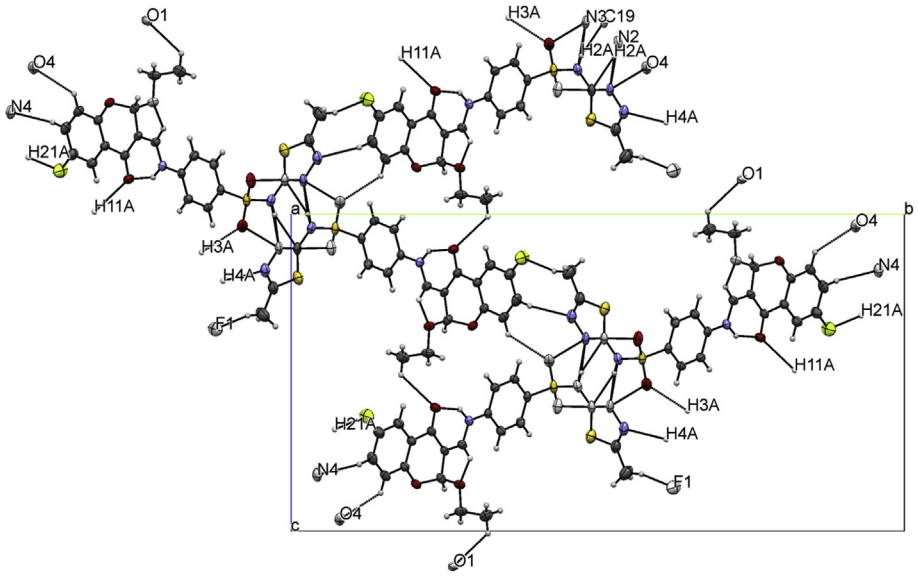

Fig. 6. Molecular packing diagram of **4a**.

as inhibitors of yet another metallophosphoesterase enzyme ecto-5′-NT (EC 3.1.3.5, lymphocyte differentiation antigen CD73) [17] for which a few inhibitors are known [18–20]. Ecto-5′-NT is anchored to the cell membrane via GPI linkages and is responsible for dephosphorylation of ribo- and deoxyribonucleotide-5′-monophosphates to corresponding nucleosides, with AMP as the preferred substrate [21]. It is over expressed in tumors and is implicated in promoting metastatic activity of tumors by increasing extracellular concentrations of adenosine [22,18]. Keeping this in mind all compounds were assayed against ecto-5′-NT (Table 3). All compounds derived from 4-ABS (**1a**–**1e**) inhibited ecto-5′-NT modestly, up to 52% of inhibition at 0.1 mM concentration. It has been found that substitution of chromone ring increases ecto-5′-NT inhibition. Among compounds derived from 3-ABS, the 6,8-dibromo compound **2d** and 6-ethyl substituted **2e** showed inhibition. Compounds derived from 2-ABS, **3a**–**3c** were devoid of any ecto-5′-NT inhibitory activity, whereas, compounds **3d** and **3e** exhibited some inhibition. The 6,8-dibromo compound **3d** showed notable 63% inhibition, whereas, the ethyl substituted **3e** did not have any effect on the ecto-5′-NT activity. Among compounds of type **B**, all were inactive except **4b** which exhibited a weak unimpressive 26% inhibition.

Table 2
Inhibition activities of chromone based sulfonamide derivatives **1a**–**1e**, **2a**–**2e**, **3a**–**3d** and **4a**–**4f** against calf intestine alkaline phosphatase, porcine kidney and bovine kidney tissue non-specific alkaline phosphatase.

Compound	$K_i \pm$ SEM (μM)[a]		
	IALP[b] (bovine intestine)	TNALP[b] (porcine kidney)	TNALP[b] (bovine kidney)
1a	90.6 ± 8.9	10.9 ± 1.8	6.8 ± 1.0
1b	1.43 ± 0.4	66.8 ± 3.0	220 ± 37
1c	0.41 ± 0.002	44.6 ± 2.9	48 ± 13
1d	5.1 ± 0.2	55.3 ± 2.5	63 ± 16
1e	2.6 ± 0.03	68.8 ± 3.0	60 ± 6.2
2a	33.5 ± 8.0	41.7 ± 8.3	41 ± 8.3
2b	17.1 ± 0.02	19.9 ± 0.1	18 ± 2.2
2c	8.7 ± 0.09	51.3 ± 1.4	44 ± 6.7
2d	0.8 ± 0.001	67.9 ± 12	26 ± 9.9
2e	2.1 ± 0.08	20.1 ± 1.2	16.8 ± 9.3
3a	0.049 ± 0.007	21.3 ± 6.3	27 ± 5.8
3b	0.78 ± 0.13	2.8 ± 0.4	43 ± 7.4
3c	0.021 ± 0.007	0.021 ± 0.002	0.13 ± 0.01
3d	0.2 ± 0.01	11.7 ± 1.2	29 ± 4.1
3e	0.4 ± 0.001	18.0 ± 1.1	29 ± 3.0
4a	0.01 ± 0.001	31.8 ± 7.6	21 ± 7.8
4b	0.085 ± 0.01	0.079 ± 0.01	0.25 ± 0.07
4c	9.3 ± 0.01	73.6 ± 6	74 ± 14
4d	0.41 ± 0.06	21.2 ± 2.1	22 ± 5.9
4e	7.8 ± 0.02	52.5 ± 3.5	38 ± 11
4f	7.8 ± 0.03	35.4 ± 1.3	23 ± 11

[a] Values are the mean ± SEM of three experiments.
[b] TNALP, tissue-non specific alkaline phosphatase; IALP, calf intestinal alkaline phosphatase.

An additional relationship can be derived from comparison of SAR of three structural isomers **1d**, **2d** and **3d**. Among all compounds analyzed in this series, **3d** is an active inhibitor of ecto-5′-NT (63% inhibition). As the position of sulfonamide group is changed from *o*- to *m*- as in **2d**, ecto-5′-NT activity decreases to 54%. When sulfonamide group is at para position (**1d**), the activity decreases even further and is only 43%. Although the decrease in inhibition is not sharp, but given the lack of ecto-5′-NT inhibitors in literature, this SAR may be exploited in hopes of optimizing inhibitors from this class of compounds. Interestingly, for the same structural isomers, the IALP inhibition activity also decreases in the same manner (Fig. 12). In our opinion it is important to assay inhibitors of ALP against ecto-5′-NT as well, since both these enzymes are widely distributed in living systems, both are AMP hydrolyzing ectoenzymes. Although the inhibition shown by these compounds is only modest, nevertheless, this information is noteworthy especially when one considers the scarcity of known ecto-5′-NT inhibitors in the available literature.

2.3. Molecular docking studies

Molecular docking studies were carried out to determine the probable binding modes of these compounds in homology modeled active sites of both the enzymes. Fig. 13 shows plausible binding modes for three representative compounds **2a**, **3a** and **4a** (XRD data for these compounds is also reported here). 3D generated models structural analyses showed that both isozymes contain similar residues in active site except with the difference of Arg-127 and Ser 447 in IALP with Gly-126 and Arg 450 in TNALP. The top ranked best

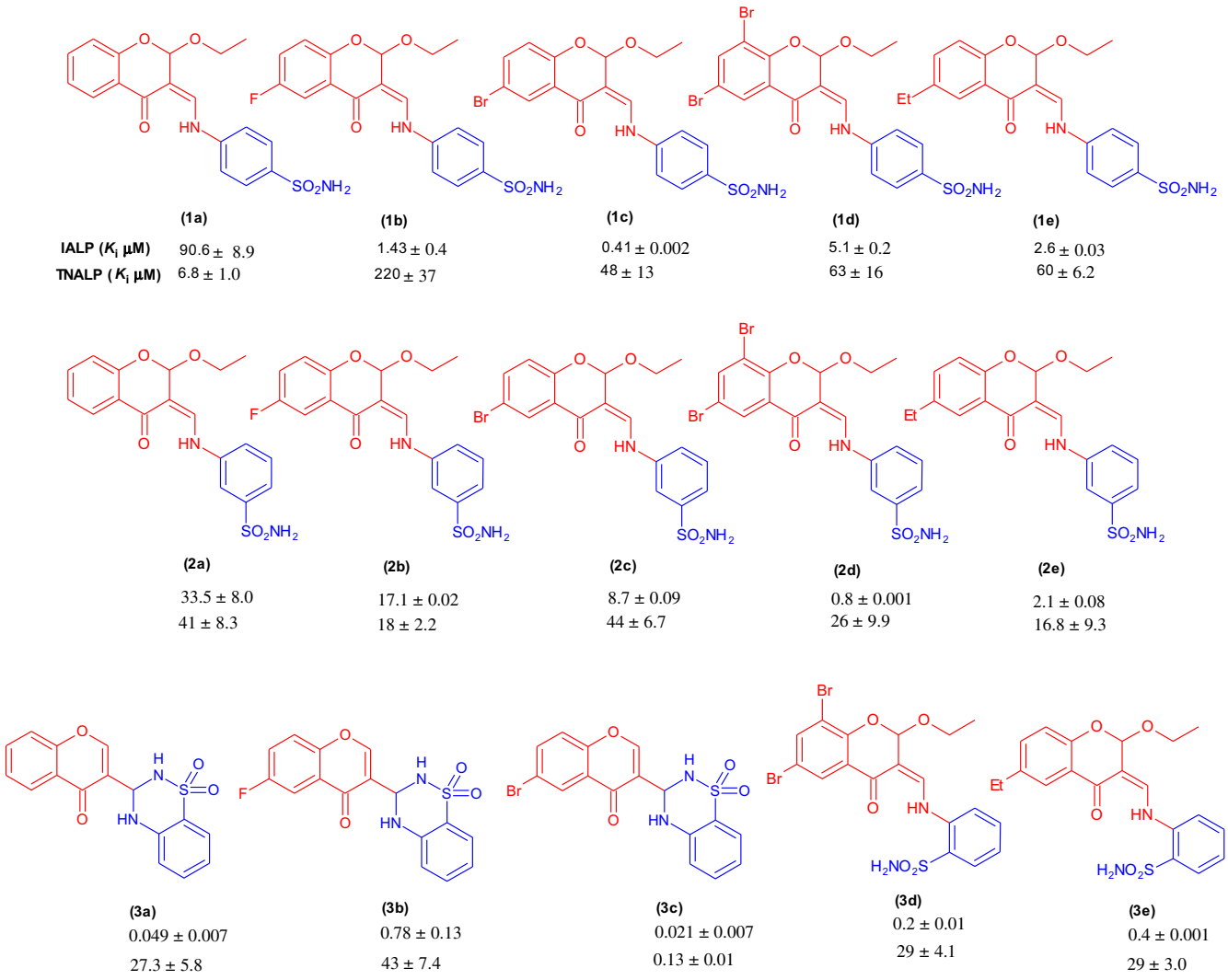

Fig. 7. Comparison of bovine IALP and bovine TNALP inhibition activities (K_i, μM) of compounds **1a**–**1e**, **2a**–**2e** and **3a**–**3e**.

probable binding mode of the most active IALP inhibitor (**4a**) is shown in Fig. 14. The sulfone group of **4a** makes strong ionic interaction with the Zn ion in active site and thiadiazole group formulates H-bonding with the Arg-127, whereas carbonyl oxygen of chromen makes H-bonding with the Arg169 present at the edge of binding site. In our modeling studies it has been observed that in IALP, most of the compounds have similar binding interaction pattern. Whereas in TNALP, the binding modes and interaction patterns are not consistent like those in IALP. This might be due to the absence of non conserved residue Arg-127 in TNALP, which is responsible for H-bonding interactions of these compounds in IALP. This difference might be the explanation for the relative selectivity of these compounds series for IALP over TNALP enzyme.

3. Conclusions

Series of novel chromone containing sulfonamides was synthesized and evaluated for their alkaline phosphatase inhibitory activity. Two major classes of ALP, i.e., tissue non specific TNALP (from bovine and porcine source) and intestinal IALP (from bovine source) were selected for enzyme assay. All compounds showed excellent and selective IALP inhibition over TNALP with K_i value up to 0.01 ± 0.001 μM. Molecular docking studies were carried out to study the selective inhibition showed by these compounds. Compounds **3c** (K_i, 0.021 ± 0.007 μM) and **4a** (K_i, 0.01 ± 0.001 μM) were found to be most active IALP inhibitors. This is the first study describing compounds based on chromone scaffold that exhibit not only potent but also highly selective IALP inhibition activities as compared to TNALP.

4. Experimental

All reagents were purchased from either Sigma or Aldrich and were used as such. Commercially available solvents were used. Ethanol was distilled and dried using standard methods and stored over molecular sieves. Reaction progress and product purity was monitored by TLC silica gel plates (0.2 mm, 60 HF_{254}, Merck). TLC spots were analyzed under short and long wavelength UV radiation. Melting points were taken on a Gallenkamp melting point apparatus and were uncorrected. Purity of compounds was established by using HPLC (Shimadzu Liquid Chromatograph LC-10 AS with UV Spectrophotometric Detector, Shimadzu SPD-6A) on C18 column (M2 Analytical column 250 × 4.6 mm; 5 μm). All the chromatograms obtained were very similar due to chemical similarity of the compounds. IR spectra were recorded on Perkin Elmer Spectrum BX-II. ^{1}H NMR and ^{13}C NMR spectra were recorded on

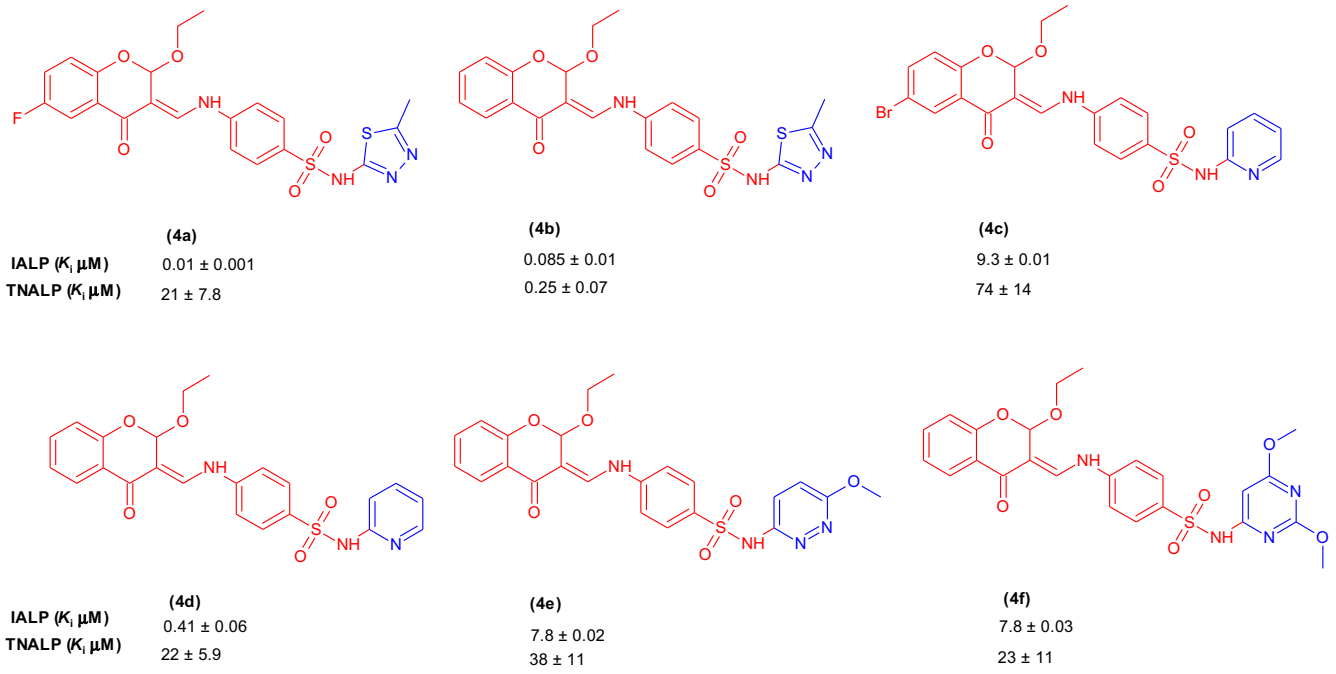

Fig. 8. Comparison of bovine IALP and bovine TNALP inhibition activities (K_i, μM) of compounds **4a**–**4f**.

Bruker (300, 400 and 500 MHz) AMX Spectrometer. Chemical shift values were referenced against TMS. DMSO-d_6 was used as solvent for NMR spectroscopy. Mass Spectra were recorded on Finnigan MAT 312 Spectrometer. Calf intestine alkaline phosphatase IALP (1000 U), porcine kidney alkaline phosphatase TNALP (100 U), Tris HCl, $MgCl_2$, $ZnCl_2$ and phenyl phosphate disodium salt were purchased from Sigma, Germany. For the spectrophotometric determination of *p*-nitrophenol which was product of ALP, a 96 well plate microplate reader from Bio-Tek ELx 800™, Instruments, Inc. USA was used.

4.1. General method for the synthesis of compounds *3a*–*3e* and *4a*–*4f*

A solution of 0.001 M 6-(un)substituted 3-formylchromone in 10 mL ethanol was stirred with heating until dissolved. Catalytic amount of *p*-toluenesulfonic acid (*p*-TsOH) was added (for compounds **3a**–**3e**) followed by the addition of equimolar solution of appropriate sulfonamide in 10 mL of ethanol. The reaction mixture was refluxed for 3.5 h and kept overnight. Solid product was obtained by filtration and purified by recrystallization from a mixture of hot ethanol and acetone (1:1).

4.1.1. 3-(1,1-Dioxido-3,4-dihydro-2H-1,2,4-benzothiadiazin-3-yl)-4H-chromen-4-one (*3a*)

Yield 65% as yellow crystalline solid, m.p. 188–190 °C; IR (ν, cm^{-1}): 1648 (C=O), 1557 (C=C), 1286 (C–O), 3343 (NH), 1154 (SO2sym), 1376 (SO2as). EI–MS *m*/*z* (rel. int. %) 326.0 (14), 263.2 (73.2), 172.0 (73.5), 121.0 (35.8), 92.1 (100), 65.0 (87.2). ^{1}H NMR (DMSO-d_6, 300 MHz) δ: 6.06 (1H, d, J = 12.0 Hz, H-8), 6.81 (1H, t, J = 7.7 Hz, H-4′), 6.85 (1H, d, J = 8.3 Hz, H-6′), 7.31 (1H, s, H-11), 7.34 (1H, ddd, J = 1.2 Hz, J = 7.9 Hz, H-5′), 7.52–7.90 (5H, m, ArH (chromone), $-SO_2NH$, NH), 8.15 (1H, dd, J = 1.2 Hz, J = 7.9 Hz, H-3′), 1H, 8.63 (s, H-2). ^{13}C NMR (DMSO-d_6, 400 MHz) δ: 174.49 (C-4), 155.63 (C-9), 143.64 (C-2′), 123.81 (C-10), 121.48 (C-1′), 120.40 (C-3), 156.82 (C-2), 134.84 (C-7), 133.06 (C-5′), 126.10 (C-5), 125.28 (C-3′), 123.81 (C-6), 118.60 (C-8), 117.11 (C-4′), 116.58 (C-6′), 60.27 (C-11).

4.1.2. 3-(1,1-Dioxido-3,4-dihydro-2H-1,2,4-benzothiadiazin-3-yl)-6-fluoro-4H-chromen-4-one (*3b*)

Yield 81% as white crystalline needles, m.p. 198–200 °C; IR (ν, cm^{-1}): 1645 (C=O), 1603 (C=C), 1288 (C–O), 3429 (NH), 1154 (SO_2^{sym}), 1376 (SO_2^{asym}). EI–MS *m*/*z* (rel. int. %) 344.0 (7), 281 (76), 190.1 (44), 164 (13), 139.1 (22), 92.1 (29), 65.1 (62). ^{1}H NMR (DMSO-d_6, 500 MHz) δ: 6.02 (1H, d, J = 9.5 Hz, H-8), 6.84 (1H, d, J = 8.3 Hz, H-6′), 6.80 (1H, t, J = 7.7 Hz, H-4′), 7.30 (1H, s, H-11), 7.353 (1H, t, J = 7.8 Hz, H-5′), 7.54 (1H, d, J = 7.8 Hz, H-3′), 7.77–7.83 (3H, m, NH, H-7, $-SO_2NH$), 7.87 (1H, dd, J = 4.2 Hz, J = 9.1 Hz, H-5), 8.65 (1H, s, H-2). ^{13}C NMR (DMSO-d_6, 400 MHz) δ: 173.88 (C-4), 160.46 (C-6), 158.02 (C-9), 152.12 (C-2′), 143.57 (C-10), 124.47 (C-1′), 119.84 (C-3),

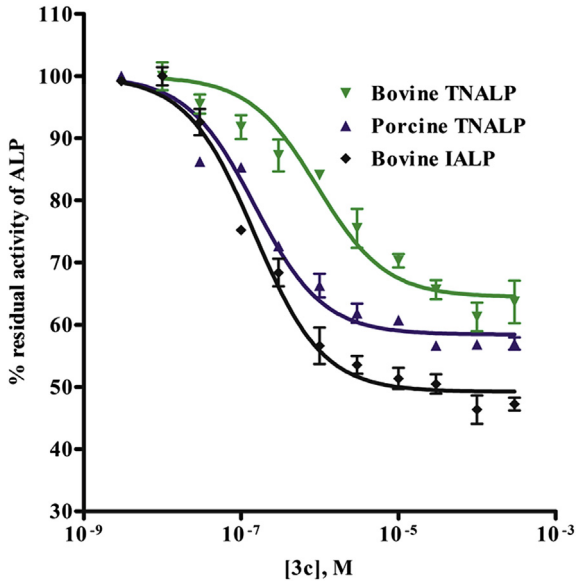

Fig. 9. Concentration-response curves of **3c** against bovine TNALP, bovine IALP, and porcine TNALP.

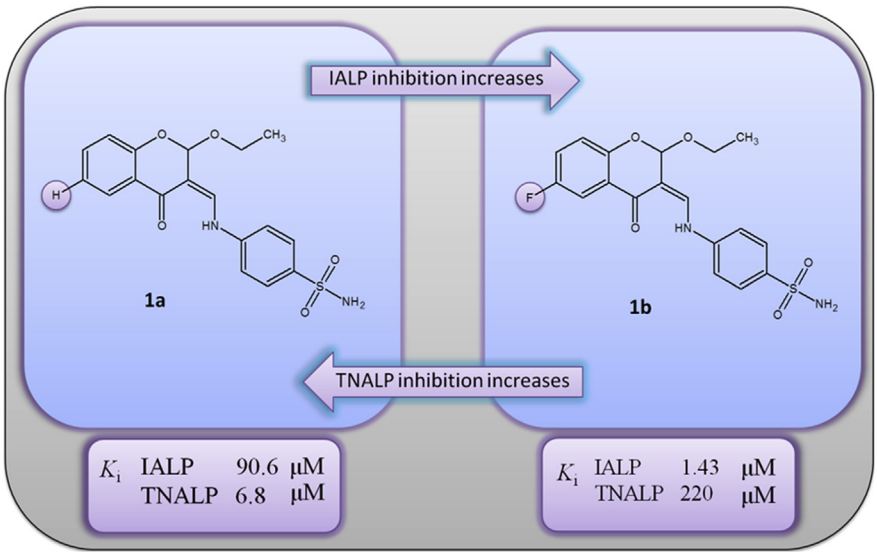

Fig. 10. 6-Substitution at chromone ring causes a decrease in bovine TNALP inhibition activity and an increase in bovine IALP inhibition.

157.10 (C-2), 133.09 (C-5′), 123.80 (C-3′), 123.17 (C-7), 121.50 (C-8), 117.17 (C-4′), 116.32 (C-5), 110.04 (C-6′), 60.18 (C-11).

*4.1.3. 6-Bromo-3-(1,1-dioxido-3,4-dihydro-2H-1,2,4-benzothiadiazin-3-yl)-4H-chromen-4-one (**3c**)*

Yield 77% as colorless needles, m.p. 224–226 °C; IR (ν, cm^{-1}): 1645 (C=O), 1602 (C=C), 1287 (C–O), 3355 (NH), 1157 (SO2sym), 1316 (SO2asym). EI–MS *m/z* (rel. int. %) 406.0 (15), 343.1 (31), 252.0 (27), 172.1 (25), 155.0 (40), 92.1 (100), 65.1 (75). ^{1}H NMR (DMSO-d_6, 400 MHz) δ: 6.02 (1H, br s, NH), 6.81 (1H, t, J = 7.6 Hz, H-4′), 6.84 (1H, d, J = 8.4 Hz, H-6′), 7.31 (1H, s, H-11), 7.35 (1H, t, J = 7.8 Hz, H-5′), 7.54 (1H, d, J = 7.6 Hz, H-8), 7.76 (1H, d, J = 7.8 Hz, H-3′), 7.84 (1H, br s, $-SO_2NH$), 8.05 (1H, dd, J = 2.4 Hz, J = 7.8 Hz, H-7), 8.20 (1H, d, J = 2.4 Hz, H-5), 8.65 (1H, s, H-2). ^{13}C NMR (DMSO-d_6, 400 MHz) δ: 173.31 (C-4), 154.61 (C-9), 143.55 (C-2′), 127.33 (C-10), 124.72 (C-1′), 120.58 (C-6), 118.54 (C-3), 157.19 (C-2), 137.49 (C-7), 133.09 (C-5), 123.80 (C-5′), 121.51 (C-3′), 121.51 (C-8), 117.19 (C-4), 116.33 (C-6′), 60.16 (C-11).

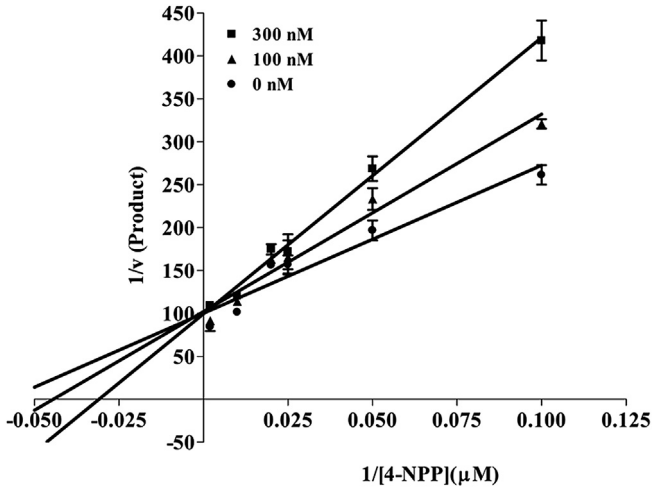

Fig. 11. Double-reciprocal plots of the inhibition kinetics of bovine intestine alkaline phosphatase by compound **3c**. Changes in the initial velocities of the reaction were measured at different concentrations of the inhibitor **3c** using substrate (4-NPP) concentrations of 0.01–1 mM.

*4.1.4. 2-{[(6,8-Dibromo-2-ethoxy-4-oxo-2H-chromen-3(4H)-ylidene)methyl]amino} benzenesulfonamide (**3d**)*

Yield 72% as yellow needles, m.p. 166–168 °C; IR (ν, cm^{-1}): 1640 (C=O), 1592 (C=C), 1280 (C–O), 3345 (NH_2), 1153 (SO_2^{sym}), 1336 (SO_2^{asym}). EI–MS *m/z* (rel. int. %) 420.1 (7), 247.0 (100), 172.0 (31), 146.0 (9), 121.1 (17), 76.1 (28). ^{1}H NMR (DMSO-d_6, 400 MHz) δ: 1.11 (3H, t, J = 7.2 Hz, CH_3), 3.77 (2H, q, J = 7.2 Hz, CH_2), 12.24 (1H, d, J = 12.4 Hz, NH), 8.14 (1H, d, J = 12.4 Hz, CH enamine), 7.90 (1H, s, H-7), 8.07 (1H, s, H-5), 6.14 (1H, s, H-2), 7.86 (1H, d, J = 7.6 Hz, H-6′), 7.77 (4H, m, $-SO_2NH_2$, ArH benzene), 7.33 (1H, m, H-4′). ^{13}C NMR (DMSO-d_6, 300 MHz) δ: 177.86 (C-4), 151.45 (C-9), 124.97 (C-2′), 113.87 (C-10), 139.42 (C-1′), 113.01 (C-6), 142.14 (C-8), 103.58 (C-3), 100.63 (C-2), 145.71 (C-7), 138.75 (C-5), 116.96 (C-5′), 116.74 (C-4′), 127.86 (C-3′), 127.44 (C-6′), 138.87 (C-11), 63.57 (CH_2 ethoxy), 14.75 (CH_3 ethoxy).

*4.1.5. 2-{[(6-Ethyl-2-ethoxy-4-oxo-2H-chromen-3(4H)-ylidene) methyl]amino} benzenesulfonamide (**3e**)*

Yield 72% as yellow needles, m.p. 166–168 °C; IR (ν, cm^{-1}): 1640 (C=O), 1592 (C=C), 1280 (C–O), 3345 (NH_2), 1153 (SO_2^{sym}), 1336 (SO_2^{asym}). EI–MS *m/z* (rel. int. %) 420.1 (7), 247.0 (100), 172.0 (31), 146.0 (9), 121.1 (17), 76.1 (28). ^{1}H NMR (DMSO-d_6, 400 MHz) δ: 1.01 (3H, t, J = 7.2 Hz, CH_3 ethyl), 1.20 (3H, t, J = 7.5 Hz, CH_3 ethoxy), 3.68 (2H, q, J = 7.2 Hz, CH_2 ethoxy), 2.65 (2H, q, J = 7.5 Hz, CH_2 ethyl), 11.81 (1H, d, J = 12.3 Hz, NH), 8.15 (1H, d, J = 12.6 Hz, H11), 7.40 (1H, dd, J = 2.4 Hz, J = 8.7 Hz, H-7), 7.53 (2H, d, J = 8.7 Hz, H-4′, H-5′),

Table 3
Percent inhibition values against human ecto-5′-NT at 0.1 mM concentration.

Compound	% inhibition Ecto-5′-NT	Compound	% inhibition Ecto-5′-NT
1a	5.7	**3b**	0
1b	16	**3c**	0
1c	52	**3d**	63
1d	43	**3e**	4
1e	13	**4a**	0
2a	0	**4b**	26
2b	0	**4c**	0
2c	0	**4d**	0
2d	54	**4e**	0
2e	30	**4f**	0
3a	0		

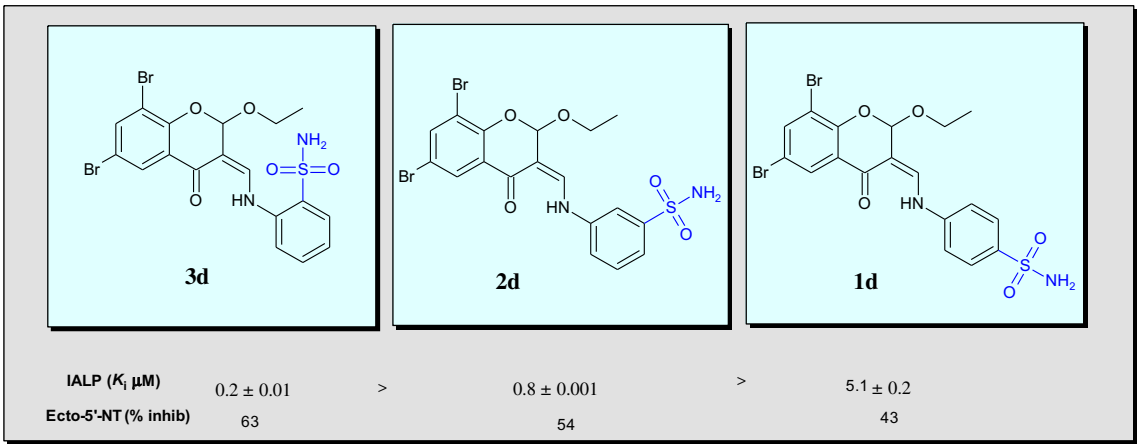

Fig. 12. IALP and Ecto-5′-NT inhibition activities for 3 structural isomers **1d**, **2d** and **3d** showing a decrease in inhibition activity as the sulfonamide group is shifted from *o*- through *m*- to *p*-position of the benzene ring.

7.01 (1H, d, J = 8.4 Hz, H-8), 7.80 (2H, d, J = 8.7 Hz, H-3′, H-6′), 7.29 (2H, br s, $-SO_2N\underline{H}_2$), 7.64 (1H, s, H-5), 5.91 (1H, s, H-2). ^{13}C NMR (DMSO-d_6, 300 MHz) δ: 180.78 (C-4), 153.87 (C-9), 138.73 (C-2′), 122.09 (C-10), 142.54 (C-1′), 137.22 (C-6), 117.99 (C-8), 105.00 (C-3), 99.84 (C-2), 134.50 (C-7), 124.18 (C-5), 63.01 (CH_2 ethoxy), 27.30 (CH_2 ethyl), 15.56 (CH_3 ethoxy), 14.95 (CH_3 ethyl), 127.57 (C-6′), 127.44 (C-3′), 116.33 (C-4′), 116.17 (C-5′), 143.91 (C-11).

*4.1.6. 4-{[(6-Fluoro-2-ethoxy-4-oxo-2H-chromen-3(4H)ylidene) methyl]amino}-N-(5-methyl-1,3,4-thiadiazol-2-yl) benzenesulfonamide (**4a**)*

Yield 62% as yellow crystalline solid, m.p. 162–164 °C; IR (ν, cm^{-1}): 1651 (C=O), 1563 (C=C), 1261 (C–O), 3338 (NH), 1136 (SO_2^{sym}), 1382 (SO_2^{asym}). EI–MS m/z (rel. int. %) 444.0 (33), 380.1 (48), 282.1 (78), 255.0 (30), 190.1 (58), 164.0 (37), 139.0 (46), 92.0 (37), 59.0 (100). ^{1}H NMR (DMSO-d_6, 400 MHz) δ: 1.08 (3H, t, J = 6.8 Hz, CH_3), 1.06 (3H, s, CH_3 thiadiazole), 3.72 (2H, q, J = 6.8 Hz, CH_2), 5.44 (1H, s, H-2), 11.76 (1H, d, J = 12.4 Hz, NH), 8.18 (1H, d, J = 12.4 Hz, H-11), 7.53 (1H, d, J = 8.8 Hz, H-3′, H-5′), 7.77 (2H, d, J = 8.8 Hz, H-2′, H-6′), 7.15 (1H, dd, J = 4.4 Hz, J = 8.8 Hz, H-8), 7.49 (1H, d, J = 8.7 Hz, H-5), 7.43 (2H, m, H-7, NH). ^{13}C NMR (DMSO-d_6, 400 MHz) δ: 63.17 (CH_2), 16.05 (CH_3), 18.53 (CH_3 thiadiazole), 179.47 (C-4), 167.80 (C-12), 158.25 (C-13), 155.88 (C-9), 154.52 (C-6), 151.89 (C-1′), 142.93 (C-4′), 136.67 (C-10), 104.59 (C-3), 144.64 (C-11), 127.55 (C-3′, C-5′), 116.83 (C-2′, C-6′), 99.93 (C-2), 121.77 (C-7), 123.01 (C-8), 110.93 (C-5).

*4.1.7. 4-{[(2-Ethoxy-4-oxo-2H-chromen-3(4H)ylidene)methyl] amino}-N-(5-methyl-1,3,4-thiadiazol-2-yl)benzenesulfonamide (**4b**)*

Yield 81% as yellow crystalline solid, m.p. 172–174 °C; IR (ν, cm^{-1}): 1650 (C=O), 1570 (C=C), 1287 (C–O), 3429 (NH), 1154 (SO_2^{sym}), 1376 (SO_2^{asym}). EI–MS m/z (rel. int. %) 426.2 (8), 362.1 (29), 172.1 (37), 92.1 (40), 76.0 (53), 65.1 (52), 59.0 (100). ^{1}H NMR (DMSO-d_6, 300 MHz) δ: 1.09 (3H, t, J = 7.2 Hz, CH_3), 1.60 (3H, s, CH_3 thiadiazole), 3.73 (2H, q, J = 7.3 Hz, CH_2), 5.94 (1H, s, H-2), 11.79 (1H, d, J = 12.3 Hz, NH), 8.14 (1H, d, J = 12.3 Hz, H-11), 7.77 (2H, d, J = 8.7 Hz, H-3′, H-5′), 7.52 (2H, d, J = 8.8 Hz, H-2′, H-6′), 7.08 (1H, d, J = 8.1 Hz, H-8), 7.154 (1H, t, J = 7.5 Hz, H-6), 7.84 (1H, dd, J = 1.5, J = 7.8 Hz, H-5), 7.56 (1H, ddd, J = 1.8, J = 7.8, H-7). ^{13}C NMR (DMSO-d_6, 300 MHz) δ: 63.08 (CH_2), 16.03 (CH_3), 18.53 (CH_3 thiadiazole), 180.61 (C-4), 167.76 (C-12), 155.72 (C-13), 154.50 (C-9), 121.96 (C-6),

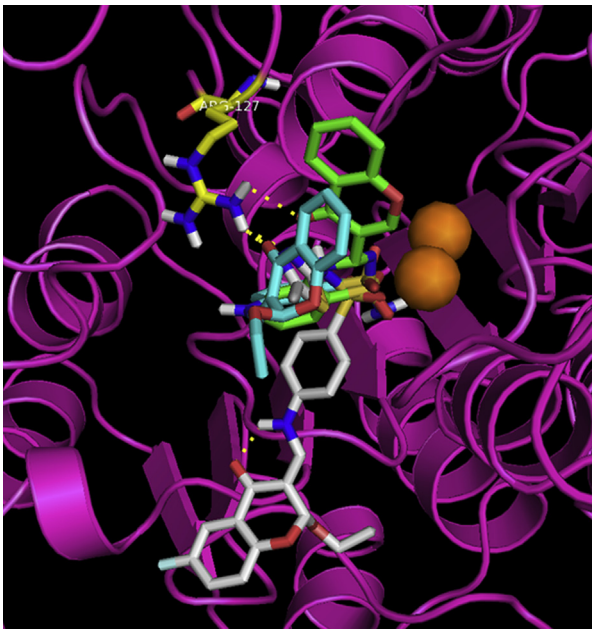

Fig. 13. Plausible binding modes for compounds **2a**, **3a** and **4a** (**2a** = cyan, **3a** = green, **4a** = white). (For interpretation of the references to color in this figure legend, the reader is referred to the web version of this article.)

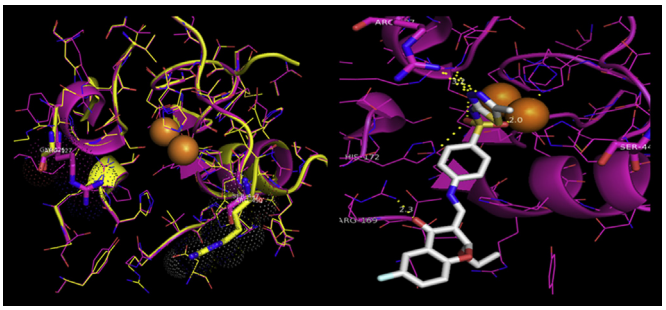

Fig. 14. Superimposed model structures of IALP (magenta) and TNALP (yellow) enzymes. Backbones are represented with cartoon and non conserved amino acids are represented with the sticks and dotted spheres. Zinc ions are shown in orange color (left). Predicted binding mode of the most active compound (**4a**) in the active site of IALP enzyme. Yellow dotted lines are showing the H-bond and ionic interactions. Distances are measured in angstroms (right). (For interpretation of the references to color in this figure legend, the reader is referred to the web version of this article.)

148.96 (C-1′), 143.34 (C-11), 143.09 (C-4′), 136.38 (C-10), 105.04 (C-3), 135.21 (C-11), 127.57 (C-3′, C-5′), 116.60 (C-2′, C-6′), 99.90 (C-2), 121.96 (C-7), 125.30 (C-8), 112.81 (C-5).

4.1.8. 4-{[(6-Bromo-2-ethoxy-4-oxo-2H-chromen-3(4H)ylidene) methyl]amino}-N-(pyridin-2-yl)benzenesulfonamide (**4c**)

Yield 70% as yellow crystalline solid, m.p. 158–160 °C; IR (ν, cm^{-1}): 1650 (C=O), 1554 (C=C), 1265 (C–O), 3352 (NH), 1158 (SO2sym), 1347 (SO2asym). EI–MS *m*/*z* (rel. int. %) 340.2 (100), 341.1 (51), 220.2 (31), 172.0 (30), 121.0 (37), 92.1 (26), 77.0 (38), 55.0 (52). ^{1}H NMR (DMSO-d_6, 400 MHz) δ: 1.08 (3H, t, J = 7.2 Hz, CH_3), 3.72 (2H, q, J = 7.3 Hz, CH_2), 5.97 (1H, s, H-2), 11.61 (1H, d, J = 12.4 Hz, NH), 8.01 (1H, br s, SO2NH), 8.25 (1H, d, J = 12.4 Hz, H-11), 7.85 (2H, d, J = 8.8 Hz, H-3′, H-5′), 7.54 (2H, d, J = 8.8 Hz, H-2′, H-6′), 7.07 (1H, d, J = 8.0 Hz, H-8), 6.88 (1H, t, J = 7.5 Hz, H-6), 7.75 (3H, m), 7.15 (2H, m). ^{13}C NMR (DMSO-d_6, 300 MHz) δ: 62.76 (CH_2), 15.84 (CH_3), 179.52 (C-4), 155.66 (C-12), 99.83 (C-13), 113.61 (C-15), 138.39 (C14), 142.85 (C-9), 135.84 (C-6), 142.96 (C-1′), 133.11 (C-4′), 122.31 (C-10), 101.95 (C-3), 143.87 (C16), 134.69 (C-11), 128.24 (C-3′, C-5′), 116.13 (C-2′, C-6′), 96.26 (C-2), 123.72 (C-7), 125.60 (C-8), 110.31 (C-5).

4.1.9. 4-{[(2-Ethoxy-4-oxo-2H-chromen-3(4H)ylidene)methyl] amino}-N-(pyridin-2-yl)benzenesulfonamide (**4d**)

Yield 78% as yellow crystalline solid, m.p. 150–152 °C; IR (ν, cm^{-1}): 1644 (C=O), 1599 (C=C), 1276 (C–O), 3345 (NH), 1157 (SO2sym), 1342 (SO2asym). EI–MS *m*/*z* (rel. int. %) 340.2 (100), 341.1 (51), 220.2 (31), 172.0 (30), 121.0 (37), 92.1 (26), 77.0 (38), 55.0 (52). ^{1}H NMR (DMSO-d_6, 400 MHz) δ: 1.08 (3H, t, J = 7.2 Hz, CH_3), 3.71 (2H, q, J = 7.3 Hz, CH_2), 5.92 (1H, s, H-2), 11.76 (1H, d, J = 12.4 Hz, NH), 8.01 (1H, br s, SO2NH), 8.11 (1H, d, J = 12.4 Hz, H-11), 7.85 (2H, d, J = 8.8 Hz, H-3′, H-5′), 7.49 (2H, d, J = 8.8 Hz, H-2′, H-6′), 7.07 (1H, d, J = 8.0 Hz, H-8), 6.88 (1H, t, J = 7.5 Hz, H-6), 7.72 (1H, dd, J = 1.5, J = 7.8 Hz, H-5), 7.55 (1H, ddd, J = 1.6, J = 7.6, H-7). ^{13}C NMR (DMSO-d_6, 300 MHz) δ: 62.96 (CH_2), 14.84 (CH_3), 180.52 (C-4), 155.66 (C-12), 99.83 (C-13), 113.61 (C-15), 138.39 (C14), 142.85 (C-9), 121.84 (C-6), 142.96 (C-1′), 134.09 (C-4′), 122.31 (C-10), 104.95 (C-3), 143.87 (C16), 134.69 (C-11), 128.34 (C-3′, C-5′), 116.33 (C-2′, C-6′), 96.26 (C-2), 121.72 (C-7), 125.60 (C-8), 112.31 (C-5).

4.1.10. 4-{[(2-Ethoxy-4-oxo-2H-chromen-3(4H)ylidene)methyl] amino}-N-(6-methoxypyridazin-3-yl)benzenesulfonamide (**4e**)

Yield 66% as yellow crystalline solid, m.p. 174–176 °C; IR (ν, cm^{-1}): 1640 (C=O), 1592 (C=C), 1284 (C–O), 3345 (NH), 1153 (SO_2^{sym}), 1336 (SO_2^{asym}). EI–MS *m*/*z* (rel. int. %) 436.2 (4), 371.2 (100), 172.0 (28), 146.1 (17), 138.1 (48), 121.1 (34), 92.0 (26), 77.0 (25), 65.1 (27). ^{1}H NMR (DMSO-d_6, 300 MHz) δ: 1.09 (3H, t, J = 7.2 Hz, CH_3), 3.37 (3H, s, $-OCH_3$), 3.71 (2H, q, J = 7.2 Hz, CH_2), 5.93 (1H, s, H-2), 11.79 (1H, d, J = 12.3 Hz, NH), 8.14 (1H, d, J = 12.3 Hz, H-11), 7.82 (2H, d, J = 8.4 Hz, H-3′, H-5′), 7.51 (2H, d, J = 8.7 Hz, H-2′, H-6′), 7.08 (1H, d, J = 8.4 Hz, H-8), 7.14 (1H, t, J = 7.2 Hz, H-6), 7.83–7.80 (1H, m, H-5), 7.55–7.51 (1H, m, H-7), 7.387–7.34 51 (2H, m, ArH pyridazine), 8.11 (1H, br s, $SO_2N\underline{H}$). ^{13}C NMR (DMSO-d_6, 300 MHz) δ: 63.07 (CH_2), 14.93 (CH_3), 15.15 ($-OCH_3$), 180.98 (C-4), 167.80 (C-12), 122.06 (C-13), 155.1 (C-15), 155.71 (C-9), 121.94 (C-6), 155.55 (C-1′), 142.93 (C-4′), 122.46 (C-10), 104.94 (C-3), 144.00 (C-11), 127.98 (C-3′, C-5′), 116.51 (C-2′, C-6′), 99.92 (C-2), 134.77 (C-7), 118.42 (C-8), 125.67 (C-5).

4.1.11. 4-{[(2-Ethoxy-4-oxo-2H-chromen-3(4H)ylidene)methyl] amino}-N-(2,6-dimethoxypyrimidin-4-yl)benzenesulfonamide (**4f**)

Yield 75% as yellow crystalline solid, m.p. 181–183 °C; IR (ν, cm^{-1}): 1639 (C=O), 1568 (C=C), 1282 (C–O), 3444 (NH), 1156 (SO_2^{sym}), 1337 (SO_2^{as}). EI–MS *m*/*z* (rel. int. %) 246.1 (14), 172.0 (12), 120.1 (26), 92.1 (31), 82.9 (100), 77.0 (12), 69.1 (17), 65.0 (37). ^{1}H NMR (DMSO-d_6, 400 MHz) δ: 1.09 (3H, t, J = 7.2 Hz, CH_3), 3.28 (6H, s, $-OCH_3$), 3.79 (2H, q, J = 7.2 Hz, CH_2), 5.95 (1H, s, ArH pyrimidine), 5.93 (1H, s, H-2), 11.75 (1H, d, J = 12.4 Hz, NH), 8.13 (1H, d, J = 12.4 Hz, H-11), 7.91 (2H, d, J = 8.8 Hz, H-3′, H-5′), 7.55 (2H, d, J = 8.8 Hz, H-2′, H-6′), 7.08 (1H, d, J = 8.0 Hz, H-8), 7.15 (1H, t, J = 7.6 Hz, H-6), 7.84 (1H, dd, J = 1.6, J = 7.6 Hz, H-5), 7.52–7.55 (1H, m, H-7), 11.48 (1H, br s, $SO_2N\underline{H}$). ^{13}C NMR (DMSO-d_6, 300 MHz) δ: 18.43 (CH_3), 55.89 (CH_2), 188.27 (C-4), 157.69 (C-9), 144.41 (C-1′), 138.78 (C-4′), 124.56 (C-10), 104.84 (C-3), 163.37 (C-11), 129.22 (C-3′, C-5′), 118.82 (C-2′, C-6′), 112.34 (C-2), 135.12 (C-7), 116.33 (C-8), 126.64 (C-5), 125.21 (C-6), 84.13 (C-13), 54.29 ($-OCH_3$), 53.59 ($-OCH_3$), 174.80 (C-14), 171.61 (C-15).

4.2. Biochemical assays

4.2.1. Alkaline phosphatase activity

Initial screening was performed at a concentration of 0.1 mM of the tested compounds. For potentially active compounds, full concentration–inhibition curves were produced. To screen putative inhibitors, activities of calf intestinal alkaline phosphatase (IALP) and tissue-non specific alkaline phosphatase (TNALP) were measured by spectrophotometric assay as previously described [23]. The reaction mixture comprised of 75 μL buffer (50 mM Tris–HCl, 5 mM $MgCl_2$, 0.1 mM $ZnCl_2$, pH 9.5) and 10 μL of the tested compound (0.1 mM with final DMSO 1% (v/v)). This mixture was incubated for 10 min after adding 5 μL of IALP (0.025 U/mL) or 5 μL of TNALP (0.5 U/mL). Then, 10 μL of substrate (0.5 mM *p*-NPP) was added to initiate the reaction and the assay mixture was incubated again for 30 min at 37 °C. The change in absorbance of released *p*-nitrophenolate was monitored at 405 nm, using a 96-well microplate reader (Bio-Tek ELx 800™, Instruments, Inc. USA). The effect on the activity of each sample containing the inhibitor was compared with the control sample (without inhibitor). The compounds which exhibited over 50% inhibition of either the calf intestinal alkaline phosphatase (IALP) or tissue-non specific alkaline phosphatase (TNALP) activity were further evaluated for determination of inhibition constants (K_i values). For this purpose 8–10 serial dilutions of each compound spanning three orders of magnitude (1 mM to 10 nM) were prepared in assay buffer and their dose response curves were obtained by assaying each inhibitor concentration against all the ALPs using the above mentioned reaction conditions. All experiments were repeated three times in triplicate. The Cheng–Prusoff equation was used to calculate the K_i values from the IC_{50} values, determined by the non-linear curve fitting program PRISM 5.0 (GraphPad, San Diego, California, USA).

4.2.2. Cell transfection with ecto-5′-nucleotidase

COS-7 cells were transfected in 10-cm plates by using Lipofectamine, as reported previously [24], with plasmids expressing ecto-5′-NT (plasmid sequence deposited to Gene Bank: DQ186653). In short, confluent cells were incubated for 5 h at 37 °C in DMEM/F-12 in the absence of fetal bovine serum and with 6 μg of plasmid DNA and 24 μL of Lipofectamine reagent. The transfection was stopped by adding the same volume of DMEM/F-12 containing 20% FBS and the cells were harvested 48–72 h later. Alkaline phosphatase (EC 3.1.3.1 from calf intestine), tissue non-specific alkaline phosphatase (TNALP) from bovine, and the tissue-specific intestinal alkaline phosphatases (IALPs) from bovine, tissue-non specific alkaline phosphatase from porcine kidney were obtained from Sigma–Aldrich, Steinheim, Germany.

4.2.3. Preparation of membrane fractions

Preparation of protein extracts was done as before [24]. Briefly, transfected cells were washed three times at 4 °C, with Tris–saline buffer, collected by scraping in the harvesting buffer (95 mM NaCl,

0.1 mM PMSF, and 45 mM Tris buffer, pH 7.5) and washed twice by centrifugation at 300 *g* for 5 min at 4 °C. Subsequently, cells were resuspended in the harvesting buffer containing 10 μg/mL aprotinin and sonicated. Nuclear and cellular debris were discarded by 10 min centrifugation at 4 °C. Glycerol was added to the resulting supernatant at a final concentration of 7.5%. Samples were kept at −80 °C until used. Protein concentration was estimated using Bradford microplate assay and bovine serum albumin was used as a standard [25].

4.2.4. CE instrumentation

A P/ACE MDQ CE system (Beckman Instruments, Fullerton, USA) was used for CE separations of substrate and product of ecto-5′-NT. UV detection system of the instrument was coupled with a diode array detector (DAD). All instrumental operations like performance, data collection and peak area analysis were performed using P/ACE MDQ software 32 KARAT (Beckman Instruments, Fullerton, USA). The temperature of sample storing unit and capillary were kept at 25 °C. An eCAP™ capillary [40 cm (30 cm effective length) × internal diameter (i.d.) 75 μm × outside diameter (o.d.) 375 μm], from Beckman Instruments, Fullerton, USA, was used to perform electrophoretic separations. The separation was performed using an applied constant voltage of 15 kV and data acquisition rate of 8 Hz. Analytes were detected at 260 nm. The capillary was conditioned by pressure washing with NaOH and water for 2 min and subsequently with buffer (25 mM sodium tetra borate buffer, pH 6.5) for 1 min.

4.2.5. Ecto-5′-nucleotidase activity assays

Ecto-5′-Nucleotidase assays were performed as reported previously [26]. Stock solutions of 10 mM of each inhibitor were prepared in DMSO. A sample of 10 μL of each tested compound and 10 μL of human ecto-5′-NT (6.94 μg/mL) protein extract was pre-incubated at 37 °C for 10 min in the presence of assay buffer (final concentration 10 mM Hepes, 2 mM $MgCl_2$, 1 mM $CaCl_2$, pH 7.4). Enzymatic reaction was initiated by the addition of 10 μL of AMP as the substrate at a final concentration of 500 μM and was allowed to proceed for 10 min at 37 °C. Enzymatic reaction was stopped by heating reaction mixtures at 99 °C for 20 min. Aliquots of 50 μL of each reaction mixture were transferred to mini CE vial and injected into the CE instrument. Under the applied conditions less than 10% of the substrate was converted into product allowing the enzyme to work at V_{max} for the time of the enzymatic assay. Adenosine concentration was determined by calculating the area under its absorbance peak at 260 nm.

4.3. Molecular docking studies

4.3.1. Homology models generation

The calf intestine alkaline phosphatase and porcine tissue non specific alkaline phosphatase sequences were threaded using LOMETS [27] threading programs, which identified other known alkaline phosphatase structures in PDB (IDs: 1ZEF, 1EW2, 1ZED, 1K7H) as possible templates. Continuous fragments were generated from these templates and were used to assemble full-length models using a modified replica-exchange Monte Carlo simulation [28] where loop regions were constructed by *ab initio* modeling. The simulation decoys were clustered using SPICKER [29] and the cluster centroids were used as the next round of I-TASSER reassembly. The structures with the lowest energy in the second round of assembly simulation were selected and full-atomic models were refined using fragment guided molecular dynamics. The lowest energy models were subjected for the molecular docking simulations of the synthesized compounds.

4.3.2. Molecular docking simulations

The molecular docking of the compounds in the generated homology models was performed using the GOLD (Genetic Optimization for Ligand Docking) program. GOLD [30] uses the genetic algorithm (GA) to search the full length of conformational flexibility of the ligands inside the protein binding site. Before docking all compounds were sketched and minimized using MMFF-94 force field implemented in MOE. Hydrogen atoms were added to both the model structures and ionization states of metals ions were fixed. For docking simulations 12 Å spherical binding site was used across the zinc ions available in the binding pocket of both the enzymes. During docking simulations the protein residues remained rigid, except Ser, Thr and Tyr hydroxyl groups, in order to optimize hydrogen bonding interactions with the docked compounds. For each solution 10 GA operations were run and best ranked solution based on the chemscore was selected for each molecule, all other parameters with their default values were used.

Acknowledgment

PhD scholarship (HEC Indigenous 5000 PhD Fellowship Program, Batch-III) given to Mariya-al-Rashida funded this research project. This work was also financially supported by COMSTECH–TWAS and German-Pakistani Research Collaboration Programme to JI. J.S.'s laboratory was supported by the Canadian Institutes of Health Research.

Appendix A. Supplementary material

Supplementary material associated with this article can be found, in the online version, at http://dx.doi.org/10.1016/j.ejmech.2013.06.015.

References

[1] J.G. Zalatan, T.D. Fenn, D. Herschlag, Comparative enzymology in the alkaline phosphatase superfamily to determine the catalytic role of an active-site metal ion, J. Mol. Biol. 384 (2008) 1174–1189.
[2] S.P. Shirazi, B. Beechey, P.J. Butterworth, The role of potent inhibitors of alkaline phosphatase to investigate the role of the enzyme in intestinal transport of inorganic phosphate, Biochem. J. 194 (1981) 803–809.
[3] L. Hessle, K.A. Johnson, H.C. Anderson, S. Narisawa, A. Sali, J.W. Goding, R. Terkeltaub, J.L. Millan, Tissue-nonspecific alkaline phosphatase and plasma cell membrane glycoprotein-1 are central antagonistic regulators of bone mineralization, Proc. Natl. Acad. Sci. U. S. A. 99 (2002) 9445–9449.
[4] D. Fraser, Hypophosphatasia, Am. J. Med. 22 (1957) 730–746.
[5] C.W. Hayes, W.F. Conway, Calcium hydroxyapatite deposition disease, Radio Graph. 10 (1990) 1031–1048.
[6] F. Moog, H.S. Glazier, Phosphate absorption and alkaline phosphatase activity in the small intestine of the adult mouse and of the chick embryo and hatched chick, Comp. Biochem. Physiol. A 42 (1972) 321–336.
[7] A.D. Care, The absorption of phosphate from the digestive tract of ruminant animals, Br. Vet. J. 150 (1994) 197–205.
[8] S. Sidique, R. Ardecky, Y. Su, S. Narisawa, B. Brown, J.L. Millan, E. Sergienko, N.D. Cosford, Design and synthesis of pyrazole derivatives as potent and selective inhibitors of tissue-nonspecific alkaline phosphatase (TNAP), Bioorg. Med. Chem. Lett. 19 (2009) 222–225.
[9] M.I. Torres, P. Lorite, M.A. López-Casado, A. Ríos, A new approach using tissue alkaline phosphatase histochemistry to identify Crohn's disease, Pathol. Res. Pract. 203 (2007) 485–487.
[10] R.B. McComb, G.N. Bowers, S. Posen, Alkaline Phosphatase, Plenum Press, New York, 1979.
[11] L. Chang, D.L. Duy, S. Mebarek, F. Popowycz, S. Pellet-Rostaing, M. Lemaire, R. Buchet, Synthesis and evaluation of thiophenyl derivatives as inhibitors of alkaline phosphatase, Bioorg. Med. Chem. Lett. 21 (2011) 2297–2301.
[12] A.I. Vovk, V.I. Kalchenko, S.A. Cherenok, V.P. Kukhar, O.V. Muzychka, M.O. Lozynsky, Calix[4]arene methylenebisphosphonic acids as calf intestine alkaline phosphatase inhibitors, Org. Biomol. Chem. 2 (2004) 3162–3166.
[13] R. Dahl, E.A. Sergienko, Y. Su, Y.S. Mostofi, L. Yang, A.M. Simao, S. Narisawa, B. Brown, A. Mangravita-Novo, M. Vicchiarelli, L.H. Smith, W.C. O'Neill, J.L. Millán, N.D. Cosford, Discovery and validation of a series of aryl sulfonamides as selective inhibitors of tissue-nonspecific alkaline phosphatase (TNAP), J. Med. Chem. 52 (2009) 6919–6925.

[14] M. al-Rashida, M.N. Tahir, S.A. Nagra, M. Imran, J. Iqbal, 4-[(Z)-(2-Ethoxy-4-oxochroman-3-ylidene) methylamino]benzene sulfonamide monohydrate, Acta Crystallogr. E65 (2009) o1818–o1819.
[15] M. al-Rashida, M. Ashraf, B. Hussain, S.A. Nagra, G. Abbas, Discovery of new chromone containing sulfonamides as potent inhibitors of bovine cytosolic carbonic anhydrase, Bioorg. Med. Chem. 19 (2011) 3367–3371.
[16] D. Ekinci, M. al-Rashida, G. Abbas, M. Şentürk, C.T. Supuran, Chromone containing sulfonamides as potent carbonic anhydrase inhibitors, J. Enz. Inhib. Med. Chem. 27 (2012) 744–747.
[17] L.F. Thomson, J.M. Ruedi, A. Glass, G. Moldenhauer, P. Moller, M.G. Low, M.R. Klemens, M. Massaia, A.H. Lucas, Production and characterization of monoclonal antibodies to the glycosyl phosphatidylinositol-anchored lymphocyte differentiation antigens ecto-5′-nucleotidase (CD73), Tissue Antigens 35 (1990) 9–19.
[18] J. Spychala, Tumor-promoting functions of adenosine, Pharmacol. Ther. 87 (2000) 161–173.
[19] R. Raza, A. Saeed, J. Leka, J. Sévigny, J. Iqbal, Identification of small molecule sulfonic acids as ecto-5′-nucleotidase inhibitors, Med. Chem. 8 (2012) 1133–1139.
[20] P. Ripphausen, M. Freundlieb, A. Brunschweiger, H. Zimmermann, C.E. Muller, J. Bajorath, Virtual screening identifies novel sulfonamide inhibitors of ecto-5′-nucleotidase, J. Med. Chem. 55 (2012) 6576–6581.
[21] Y. Misumi, S. Ogata, K. Ohkubo, S. Hirose, Y. Ikehara, Primary structure of human placental 5′-nucleotidase and identification of the glycolipid anchor in the mature form, Eur. J. Biochem. 191 (1990) 563–569.
[22] L. Wang, X. Zhou, T. Zhou, D. Ma, S. Chen, X. Zhi, L. Yin, Z. Shao, Z. Ou, P. Zhou, Ecto-5′-nucleotidase promotes invasion, migration and adhesion of human breast cancer cells, J. Cancer Res. Clin. Oncol. 134 (2008) 365–372.
[23] J. Iqbal, An enzyme immobilized microassay in capillary electrophoresis for characterization and inhibition studies of alkaline phosphatases, Anal. Biochem. 414 (2011) 226–231.
[24] J. Lecka, M.S. Rana, J. Sévigny, Inhibition of vascular ectonucleotidase activities by the pro-drugs ticlopidine and clopidogrel favours platelet aggregation, Br. J. Pharmacol. 161 (2010) 1150–1160.
[25] M.M. Bradford, A rapid and sensitive method for the quantitation of microgram quantities of protein utilizing the principle of protein–dye binding, Anal Biochem. 72 (1976) 248–254.
[26] J. Iqbal, D. Jirovsky, S.Y. Lee, H. Zimmermann, C.E. Müller, Capillary electrophoresis-based nanoscale assays for monitoring ecto-5′-nucleotidase activity and inhibition in preparations of recombinant enzyme and melanoma cell membranes, Anal. Biochem. 373 (2008) 129–140.
[27] S.T. Wu, Y. Zhang, LOMETS: a local meta-threading-server for protein structure prediction, Nucleic Acids Res. 35 (2007) 3375–3382.
[28] S. Wu, J. Skolnick, Y. Zhang, Ab initio modeling of small proteins by iterative TASSER simulations, BMC Biol. 5 (2007) 17.
[29] Y. Zhang, J. Skolnick, SPICKER: a clustering approach to identify near-native protein folds, J. Comput. Chem. 25 (2004) 865–871.
[30] G. Jones, P. Willett, R.C. Glen, A.R. Leach, R. Taylor, Development and validation of a genetic algorithm for flexible docking, J. Mol. Biol. 267 (1997) 727–748.